(RESEARCH ARTICLE)

Analytical and numerical study of hot rolling railway rail sections with the help of simulation and finite element software

Iman Ahmedy [1, *] and Jamshid Nasiri [2]

[1] Civil Engineering Department, Tehran Azad Science and Research Branch, Tehran, Iran.
[2] Civil Engineering Department, Islamshahr Azad University, Tehran, Iran.

Abstract

Hot rolling of sections is one of the metal forming processes used to shape materials into profiles with a fixed cross-section, such as road rails. Iron is chosen for this process due to its repeatability. Despite the numerous equipment and high costs associated with it, the analysis of this process and its simulation can be highly desirable. In this process, the initial raw piece is passed through several rollers until the desired section's shape is created (1,2). The more passes are made, the greater the reduction in the cross-sectional area, and the tolerances increase. During rail rolling, several key factors play a crucial role, including the length of the workpiece, cross-section change, piece deviation, roller speed, and friction. This article focuses on investigating the effective parameters in this process using simulation software. For the rolling analysis, we use an isothermal and rigid model of rollers, considering the heat transfer between the rollers and the rail during the shaping process. The analysis is performed using thermal stress solutions in Abaqus/explicit. Additionally, the workpiece may deviate due to the asymmetry of the top and bottom shapes. Hence, we examine the effects of the friction coefficient between the part and the rollers on rail deflection, stress values, strain, and rolling force. The results indicate that the maximum stress on the rail's surface occurs below the points of contact with the rollers, leading to a higher percentage reduction.

Keywords: Rail; Simulation; Section; Hot rolled; Vibration

1. Introduction

Rolling a cross-section involves shaping the cross-sectional surface of the workpiece by passing it through grooves on the side surface. The rollers on a rolling rack are designed in a way that, at each stage of rolling, the shape of the cross-section of the workpiece resembles the shape of the caliber created between the grooves of the upper rollers. One of the most crucial aspects in the design of the rolling stages is the examination and recognition of how well the metal aligns within the caliber of the shaper (3,4). Various methods, such as modeling with plastic materials and advanced analysis of metal alignment using techniques like slip lines and upper limits, have been studied to understand plasticity. During the continuous hot rolling of billets through different stages, it is essential to carefully ensure that acceptable dimensions are transformed into products, and the cross-sectional area of the piece gradually decreases. Researchers in the field of hot rolling section analysis consistently strive to identify events that occur in the cross-section of the part during the exit process (5). Defining the caliber and designing the profile of the piece is of utmost importance. The application of the finite element technique in the rolling process allows us to easily study other calibers with different shapes. In rolling, various factors are considered, including material flow, resulting stresses, friction, the force applied to the rollers, temperature, and the phenomenon of roller flattening (6).

In this article, we use Abaqus software to simulate the rolling of iron rails, with a specific focus on the first two stages within a series of rolling stages.

2. Material and methods

2.1. The hot rolling process of railway rails

In this process, the preform, intended to be placed between two shaped rollers, is heated and then rolled. The standard rail has a distinct cross-section, consisting of three parts: Sir Rail, John Rail, and its base. The rail form used in this article is selected from the general classes of rail design, closely resembling an inverted T. The shape, dimensions, and standard of the sample used for rolling in this article are sourced from Harmer Steel factory, one of the manufacturers of various railway rails, and are illustrated in Figure 1.
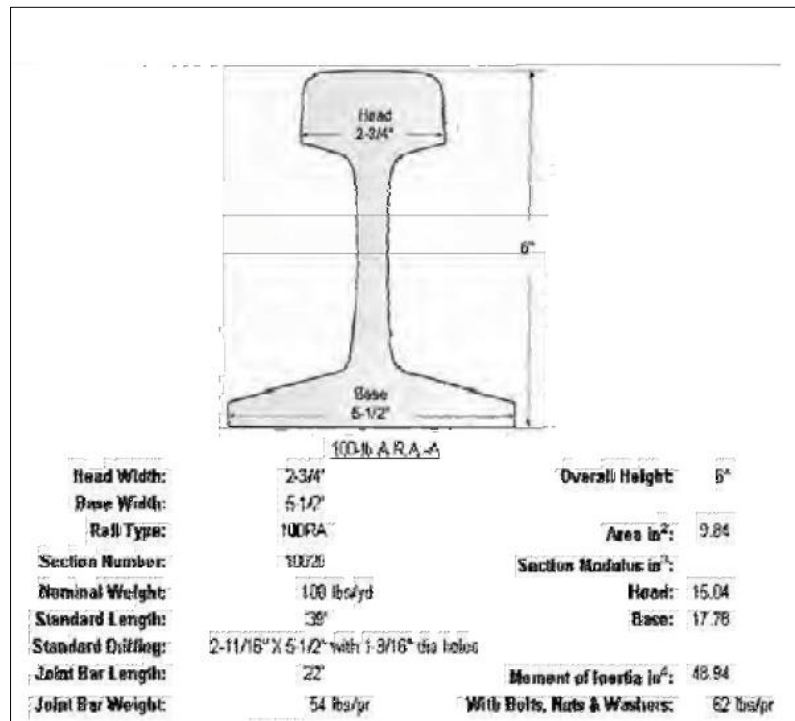

Figure 1 Exact dimensions of the rail after final rolling

The material used to simulate the rail is 309 steel, and the dimensions of the rail before the two final rolling stages are provided in Table 1.

Table 1 Rail dimensions before rolling

Thickness of the Rail Web	Seismic Zone	Rail Height	Rail Width
28 mm	76 mm	167.2 mm	130 mm

In addition, both calibers use grooved steel rollers with a diameter of 580 mm and a speed of 9 rad/s, along with smooth rollers with a speed of 16 rad/s and a diameter of 290 mm to simulate the last two stages, i.e., stages 12 and 13, at a temperature of 1100 degrees Celsius. Typically, the cross-section of rails is created from rectangular ingots and varies based on design type and rail class throughout the 10 to 18 rolling stages. Production proceeds with careful caliber design, and the rolling operations are closely monitored to ensure the produced rails meet precise dimensions and high-quality standards. Following complete rolling, the rails undergo controlled cooling, typically on cooling beds, where they are cooled to a temperature of 725 degrees Celsius. Subsequently, the rails are transferred to carrier beds, and the cooling process continues for up to 10 hours. After cooling, final operations include inspection, chamfering, and grinding of rail heads. Ultimately, the rails undergo hardening and are quenched in oil before being subjected to further heat treatment. Rails are formed using two main methods: the tab method and the grooved roller method, as well as the

angular method, and occasionally a combination of these methods is employed. As illustrated in the figure, the method employed in this article corresponds to the first method, as depicted in Figure 2. This method utilizes two grooved rollers aligned on the same axis and one tongue roller with its axis perpendicular to the two axes of the rollers.
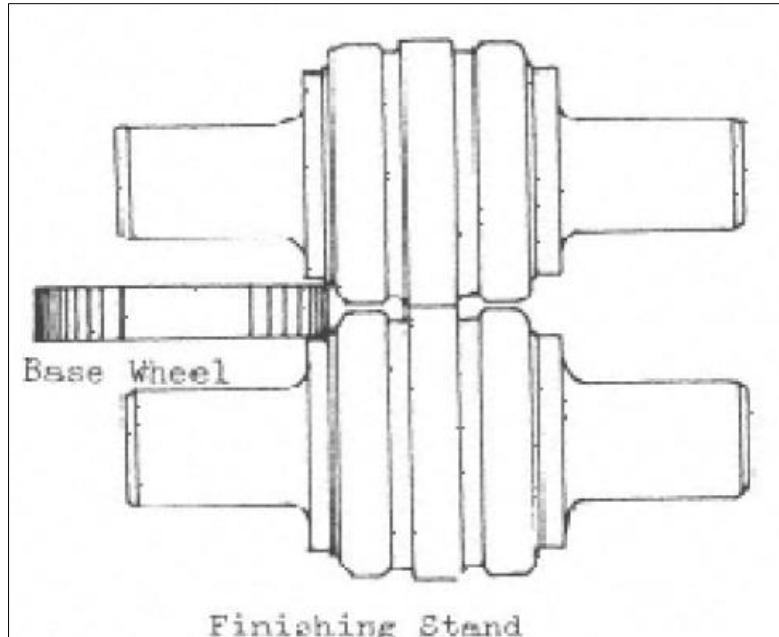
Figure 2 Design of grooved and tongued rollers

2.2. Rolling process simulation

For finite element simulations, we utilize the ABAQUS software program, known for its proficiency in analyzing nonlinear behaviors involving extensive elastic and plastic deformations. Kamyab Moghaddam addressed the critical issues of railway ground-borne vibration induced by high-speed and intercity trains, presenting a significant challenge for railway systems. His work highlighted the efficacy of vibration attenuation at the source, incorporating elastic layers beneath various track components. Kamyab Moghaddam's findings underscored the importance of the deflection and stress control method as a significant approach to reducing vibrations at the source. The current article builds on his previous work, focusing on investigating the key parameters in this process using simulation software to examine the impact of the friction coefficient between the part and the rollers on rail deflection, stress values, strain, and rolling force to control the vibration. The results affirm these findings and are compared to those obtained in Kamyab Moghaddam's previous work for validation (7). In the analysis of each stage of rolling, the rollers are considered as isothermal, and the object is modeled as rigid. Heat transfer occurs between the rollers and the rail (8,9). Heat can be generated during rolling for two reasons: plastic work done and friction caused by the contact between the roller and the workpiece. The heat lost from the rolling rail due to cooling in the environment and the use of coolant is calculated as conduction in boundary conditions, and part of the heat is radiated to the surrounding environment. Therefore, the analyses are based on the complete combination of thermal stress explicitly. In the simulation analysis, automatic adaptive meshing for the rail is used during rolling analysis to maintain the best mesh quality while changing shape. To increase the efficiency of analysis calculations, it is automatically carried out until a steady state is achieved. Conditions and criteria are applied to attain a stable state, which is based on the torsional torque of rigid rollers, an increase in the width, and plastic strain in the cross-section of the piece.

The design of two simulated calibers, our pre-final and final calibers, is shown in Figure 3.
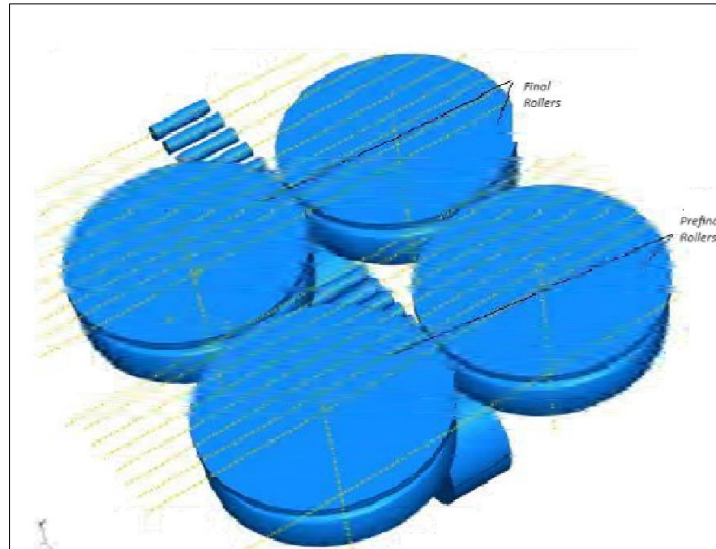
Figure 3 Two pre-final rollers and two final rollers

3. Finite element analysis

By employing the boundary element method, the shape inside the caliber is divided into different cells or elements. The subsequent pattern of shape change can be predicted through the analysis of these elements, allowing for a complex section to be anticipated. The finite element model used in the design and verification of calibers offers the advantage of analyzing the new caliber without the need for creating a complex and time-consuming model. Due to the lengthy calculation times and the complexity of mechanical and thermal boundary conditions involved in the finite element model, its application in today's rolling processes is primarily limited to evaluating analytical models and conducting preliminary studies of new calibers. During sample rolling experiments, the temperature of the input cutoff exceeds 1100 degrees Celsius, while the temperature of the rollers surpasses 150 degrees Celsius, resulting in heat transfer between the workpiece and the rollers. However, due to the high speed of the rollers, the range of heat transfer within a short time frame is limited. As a consequence, the temperature difference of the test piece from the time of entry to the exit is less than 30 degrees Celsius. Consequently, we consider this process as isothermal in our simulation.

The analysis of the stages used to model the two stages of rolling is as follows:

- The first rolling process is implemented in explicit mode to achieve a stable solution state.
- Two-dimensional meshes of the cross-sectional area for data transformation in a stable plane are generated using CAE. The final temperatures of the stable plate are also determined.
- A new cross-sectional model with finer meshes is created in CAE. In the second thermal analysis, the Abaqus/Standard subprograms are utilized to transfer heat from the previous step to the new finer meshes. The focus of the analysis is solely on heat transfer to the new meshes.
- The 3D meshes for the second rolling are generated using the new cross-sectional meshes and the thermal information from the previous stage.
- The second rolling step is performed in explicit mode to establish a stable rolling solution

3.1. Thermal analysis

The meshing for the internal heating system analysis is derived from the database outputs of the first rolling pass using CAE.

This program is used to create a temperature map for the three-dimensional analysis of the primary rolling pass and the heat transfer within the inner pass of meshes. Subsequently, more precise transverse section analysis is conducted for the second stage. To draw the temperature map for the first heat transfer analysis, the new heating mesh is employed for the second transfer analysis. The new mesh for the second heat transfer analysis is generated using the original CAE document. This program takes the database output from the first heat transfer analysis as input, examines the meshes, and produces the components of that mesh. These components are not new; they are adapted to fit the requirements of the new mesh for the second heat transfer analysis. Since the position of the nodes in the new two-dimensional mesh

differs from the position of the nodes in the internal heat transfer analysis mesh used previously, temperatures are assigned to the new mesh nodes accordingly. Abaqus/Standard heat transfer analysis employs the following modeling techniques for this purpose.

The final temperatures from the second heat transfer analysis serve as the initial temperatures for the second rolling pass. This process can also be automated using the initiator file method. Similarly, the second rolling pass is conducted in a manner similar to the first rolling pass and will conclude once it reaches a stable state (10,11).

Both experience and experiments have demonstrated that the stress in metals is dependent on the strain rate. In other words, when the strain rate increases, the stress in the metal also increases. Similar to the stress-strain relationship, there is an exponential correlation between shear stress and strain rate, represented by equation 1.

$\sigma = C \, \acute{\epsilon}m$ (1)

The constant C represents the material's resistance coefficient, while the constant m represents the material's strain rate. The values of C and m specific to the sand type discussed in this article are provided in Table 2.

Table 2 m and c values for the rail

m	c	m	c	strain	strain rate per second
1200		800			200-520
0.184	60	0.079	272	0.25	
0.174	66	0.074	311	0.4	
0.185	66	0.076	323	0.6	

3.2. Friction in hot rolling

Determining the friction coefficient in hot rolling is undoubtedly of paramount importance in practice. This is because various factors such as the quality, surface condition, dimensions, and temperature of the workpiece, as well as the surface quality and diameter of the roller, rolling speed, and more, all affect the magnitude of the friction coefficient in rolling. Due to the complexity of these factors, it is challenging to find a single formula that comprehensively encompasses all of these structural elements.

Most of the available relationships used to determine the base friction coefficient rely on experimental and laboratory data, and each of them is applicable under specific rolling conditions. One of the most significant and successful relationships for determining the friction coefficient in hot rolling of steel sections is a formula in which the friction coefficient depends on rolling temperature, roller type, and rolling speed. This relationship is formulated as follows:

$\mu = ar \, kr \, (1.05 - 0.0005)$ (2)

θ represents the rolling temperature in degrees Celsius, while ar is a constant whose magnitude varies depending on the type of roller. Different values of ar are listed in Table 3.

Table 3 Different amounts of ar

Different amounts of ar	
1	Rough steel and cast-iron rollers
0.8	Smooth steel rollers
0.55	Transparent steel rollers

kr is a constant whose magnitude is determined by the linear speed of the working rollers. According to Equation 2, the friction coefficient is calculated to be 0.3.

3.3. Calculation of roll pressure in hot rolling of steel by Gle Chi method

In this method, the average pressure of the roll in hot rolling is also as The product of a factor greater than one in the yield stress of steel Hot work conditions are suggested, in such a way that:

Pm = 2k (1 + µ C v0/25 ld / hm)   (3)

In this equation, vr represents the linear speed of the roller in meters per second, µ stands for the coefficient of friction between the workpiece and the roller, and C is dependent on the ratio of the length to the average thickness of the workpiece, which has been determined as 6. ld corresponds to the contact length of the roller, calculated based on Equation 4 (12,13). Additionally, hm refers to the average height of the part, measuring 55 mm, and Δh represents a decrease in thickness, which is 7 mm.

Ld = √R.Δh   (4)

2k represents the yield stress of steel under hot working conditions. According to the von Mises yield criterion, 2k is equal to Y1.15, which has been calculated for the specific type of steel being used. The main characteristics of this criterion are:

No preconditions are required between the main stress components. It can be formulated in terms of the first and second invariants of the stress tensor. Laboratory experience has shown that this criterion accurately predicts material behavior more effectively than the COD delivery standard.

3.4. Calculation of force in hot rolling

The determination of force in hot rolling is closely related to the determination of pressure, particularly the average pressure on the roll. If pm represents the average pressure on the roller during contact, simply multiplying it by the contact surface area yields the rolling force, as expressed in Equation 5, which is as follows:

F/Wm = Pm.√R.Δh   (5)

Where Wm is the average width of the workpiece. The average pressure, pm, is calculated using Equation 3.

The force entering the first and second pair of rollers was calculated by the software and is shown in Figures 4 and 5, respectively. As can be seen, the amount of force in the first pair of rollers is 5.44 * 10 ^6 N and for the second pair of rollers is 6.1 * 10 ^6 N, and The reason that the amount of force in the second pair of rollers is more is that The temperature in the work piece is reduced and so is the strain hardness of the piece increase.
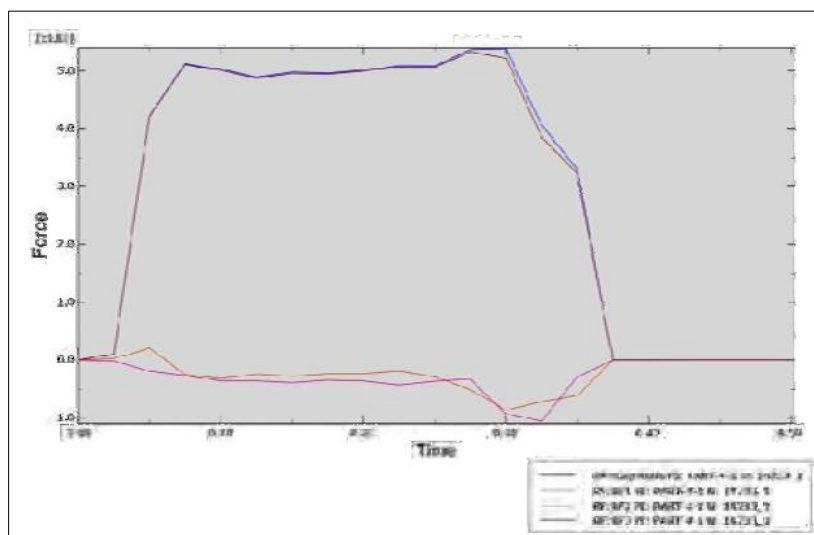

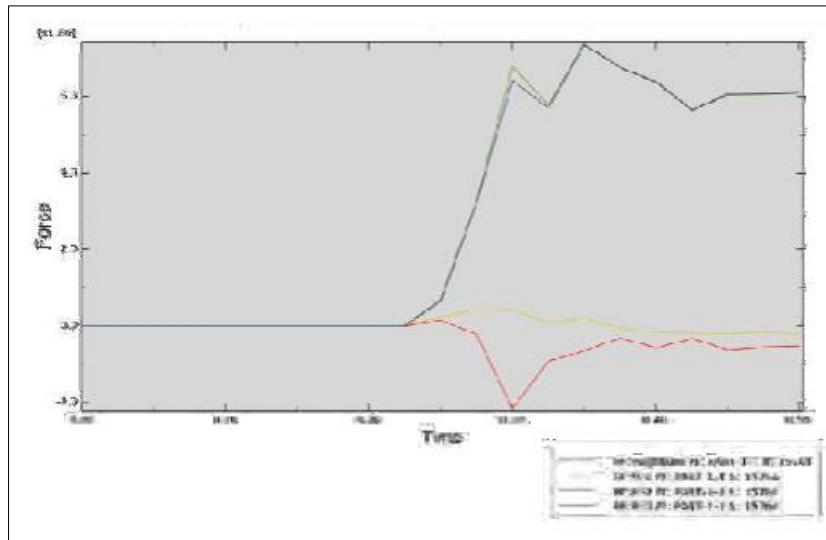**Figure 4** Two pre-final rollers and two final rollers

Figure 5 The diagram of the rolling separation force in the second pair of rollers

3.5. Deviation of the work piece up or down

If the diameter of the upper roller is larger than that of the lower roller, with both rollers rotating at the same speed, the linear speed of the upper roller becomes greater. Consequently, when the workpiece exits the gap between the two rollers, it deviates downward. This rolling condition is referred to as 'low zinc.

When forming the workpiece in a caliber that has a deep groove on one of its rollers, it results in speed differences between the material at the bottom of the groove compared to the material in areas above the groove. This discrepancy is due to the different radii of the roller for these two material regions. As a result, the workpiece may encounter difficulties when exiting the caliber, making it advisable to avoid designing calibers with excessive depth (14).
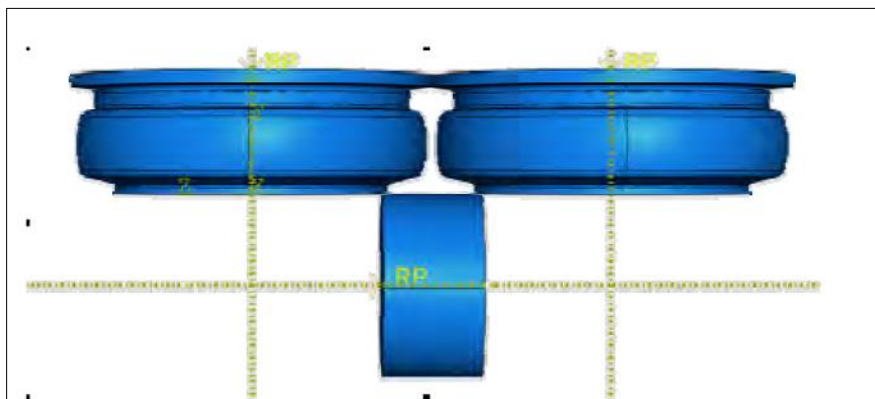

Figure 6 Use of three-roller rolling machine to prevent rail deviation

In rolling sections, the vertical movement or position of the caliber within the space between the two rollers can result in a difference in the working diameter of the upper and lower rollers (15). Aside from the roller diameters, several other factors can also cause the workpiece to move either upwards or downwards. These factors include differences in the rotational speed of the upper and lower rollers, variations in temperature between the upper and lower surfaces of the workpiece, or discrepancies in friction between the upper and lower rollers (16,17). In this article, initially, a single double-grooved roller was used, which, due to the asymmetry of the grooves around the piece's axis, caused deviation. To resolve this issue, a three-roller setup was employed, consisting of two rollers with symmetrical groove shapes and one smooth roller to shape the rail floor. The radius of the smooth roller is half that of the grooved rollers, and its rotational speed is twice as fast at 18 rad/s. When the linear speed of all the rollers was equal, deviation in the rail was observed again, as shown in Figure 7a. To eliminate the deviation, the speed of the smooth roller was reduced from 18 to 16, effectively solving the problem, and the rail was rolled without deviation. The resulting shape of the rail is depicted in Figure 7.
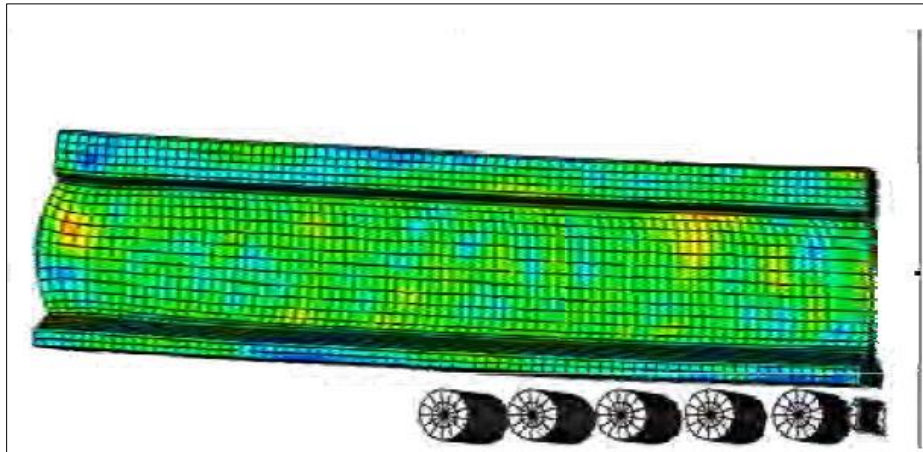
Figure 7.A Deviation to the top of the rail when the speed is the same your roll
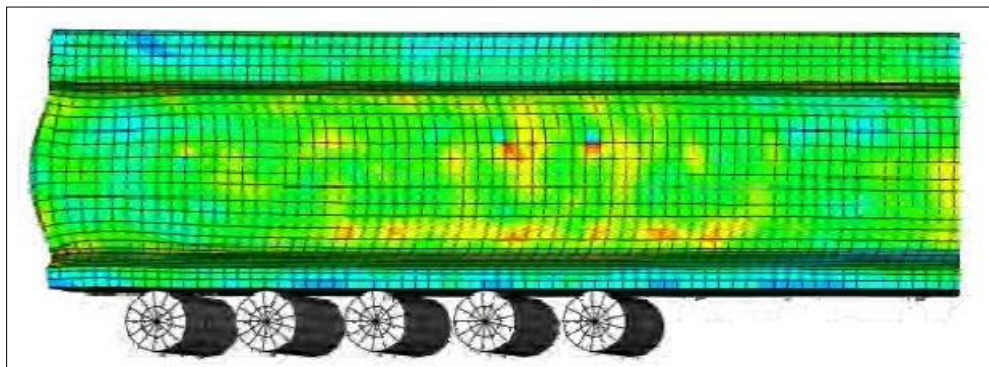

Figure 7.B Rolled rail without deviation

4. Results and discussion

The first rolling stage, which ends when the rolling conditions are deemed stable, reduces the required analysis time, while maximizing the tension in both calibers within a single plane. This plane lies under the contact point of the roller, as illustrated in Figure 8.

The analysis results reveal a uniform shape change in a stable condition, as shown in Figure 8. The region with the largest plastic strain experiences the most significant shape change. The plastic deformation leads to heat generation, with the temperature peak precisely corresponding to the location of the plastic strain peak.

As the workpiece passes between the rollers, it undergoes cooling, and its thermal gradient decreases. After the second rolling pass, it appears that stable conditions have been achieved, allowing for a significant shape change, and most of the rail's shape can be recreated by rolling with new calibers. The software used in this article cannot account for elastic shape changes, only plastic deformation and heat transfer. In multi-machine rolling, to validate the accuracy of this finite element simulation, elastic-plastic rolling in both isothermal and non-isothermal conditions within the rolling groove was conducted. A very small difference of about 0.02% was observed. Therefore, two-machine rolling analysis can be performed under isothermal conditions. Additionally, the theoretical average pressure of the first pair of rollers was calculated using Equation 3, and these results were used to calculate the theoretical force using Equation 5, with the results presented in Table 4.

Table 4 The amount of power in theory and simulation relationships

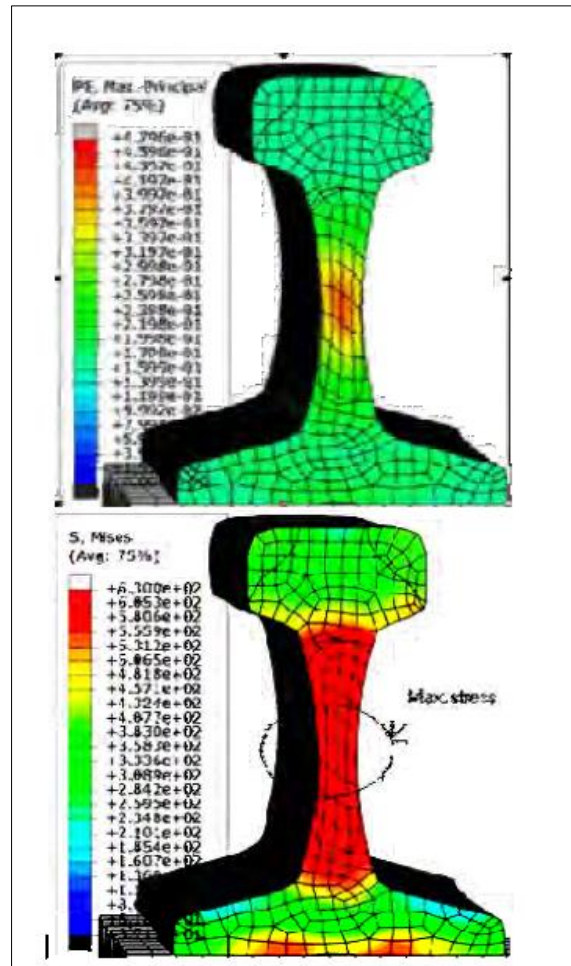| average pressure In the theory relationships (Mpa)	The rolling force in Theoretical relationships (MN)	The rolling force in Simulation (MN)
761.7	5.65	5.44

Figure 8 The maximum amount of stress and plastic shape change in the stage the end of rolling the rail

Upon comparing the theoretical relationships with the force obtained from the simulation, a difference of 3.7% was observed.

5. Conclusion

The hot rolling process in a steady state has been analyzed using ABAQUS software. In this rolling process analysis, the constant friction coefficient was employed with three rollers, two of which are coaxial, while the other is positioned vertically on the axis of the two coaxial rollers. The latter two were designed to be rigid. The simulation was carried out until a suitable response was achieved after forming. The analysis involved calculating stresses and strains in the workpiece as well as the separating force in the rollers. These calculations can serve as the foundation for further analyses.

In addition, we determined the stress and strain levels, as well as their respective locations of maximum occurrence. The workpiece's deviation during rolling was thoroughly investigated, and to mitigate it, the speed of the smooth roll was reduced. In our calculations, we observed that the forces from theoretical calculations and simulation results were in good agreement, with an error calculated at 3.7%. The outcomes of this research can be applied to simulate the rolling of rail sections and improve the shape to better match reality.

Compliance with ethical standards

Disclosure of conflict of interest

The authors has no conflict of interest in this study.

References

[1] Clark R. Rail flaw detection: overview and needs for future developments. NDT & E International. 2004 Mar 1;37(2):111–8.

[2] Bruzelius K, Mba D. An initial investigation on the potential applicability of Acoustic Emission to rail track fault detection. NDT & E International. 2004 Oct 1;37(7):507–16.

[3] Shabana AA, Zaazaa KE, Escalona JL, Sany JR. Development of elastic force model for wheel/rail contact problems. Journal of Sound and Vibration. 2004 Jan 6;269(1):295–325.

[4] Wu TX, Thompson DJ. On the impact noise generation due to a wheel passing over rail joints. Journal of Sound and Vibration. 2003 Oct 23;267(3):485–96.

[5] Kakudate S, Shibanuma K. Rail deployment and storage procedure and test for ITER blanket remote maintenance. Fusion Engineering and Design. 2003 Jan 1;65(1):133–40.

[6] Mackett R, Babalik Sutcliffe E. New urban rail systems: a policy-based technique to make them more successful. Journal of Transport Geography. 2003 Jun 1;11(2):151–64.

[7] Kamyab Moghaddam A. A Review on the Current Methods of Railway Induced Vibration Attenuations. International Journal of Science and Engineering Applications. 2017;6(4):123–8.

[8] Quinet E. Short term adjustments in rail activity: the limited role of infrastructure charges. Transport Policy. 2003 Jan 1;10(1):73–9.

[9] Xia F, Cole C, Wolfs P. The dynamic wheel–rail contact stresses for wagon on various tracks. Wear. 2008 Oct 30;265(9):1549–55.

[10] Plu J, Bondeux S, Boulanger D, Heyder R. Application of fracture mechanics methods to rail design and maintenance. Engineering Fracture Mechanics. 2009 Nov 1;76(17):2602–11.

[11] Liu HP, Wu TX, Li ZG. Theoretical modelling and effectiveness study of rail vibration absorber for noise control. Journal of Sound and Vibration. 2009 Jun 19;323(3):594–608.

[12] Tournay HM. A future challenge to wheel/rail interaction analysis and design: Predicting worn shapes and resulting damage modes. Wear. 2008 Oct 30;265(9):1259–65.

[13] Li W, Xiao G, Wen Z, Xiao X, Jin X. Plastic deformation of curved rail at rail weld caused by train–track dynamic interaction. Wear. 2011 May 18;271(1):311–8.

[14] Yoon HJ, Song KY, Kim JS, Kim DS. Longitudinal strain monitoring of rail using a distributed fiber sensor based on Brillouin optical correlation domain analysis. NDT & E International. 2011 Nov 1;44(7):637–44.

[15] Gullers P, Andersson L, Lundén R. High-frequency vertical wheel–rail contact forces—Field measurements and influence of track irregularities. Wear. 2008 Oct 30;265(9):1472–8.

[16] Xie G, Iwnicki SD. Calculation of wear on a corrugated rail using a three-dimensional contact model. Wear. 2008 Oct 30;265(9):1238–48.

[17] Belotserkovskii PM, Pugina LV. The rolling of a wheel along a corrugated rail. Journal of Applied Mathematics and Mechanics. 2008 Oct 1;72(3):288–95.